Electronic Supplementary Material (ESI) for ChemComm.

Cu Single-Atoms Embedded in Porous Carbon Nitride for Selective Oxidation of Methane to Oxygenates

Bo Wu, Ruoou Yang, Lei Shi, Tiejun Lin, Xing Yu, Ming Huang, Kun Gong, Fanfei Sun, Zheng Jiang, Shenggang Li, Liangshu Zhong,* Yuhan Sun*

1 Experimental Section

1.1 Materials.

All reagents were used as received without further purification. Melamine and cobalt (II) chloride trihydrate ($CoCl_2 \cdot 6H_2O$) were purchased from Sinopharm Chemicals. Cyanuric acid, copper (II) chloride dihydrate ($CuCl_2 \cdot 2H_2O$), iron (III) chloride hexahydrate ($FeCl_3 \cdot 6H_2O$), manganese chloride tetrahydrate ($MnCl_2 \cdot 4H_2O$) were purchased from Aladdin Chemicals. All the agents without further purification.

1.2 Synthesis of M-SAs/C_3N_4 and C_3N_4.

Taking Cu-SAs/C_3N_4 as an example, 2.557 g (15 mmol) $CuCl_2 \cdot 2H_2O$ and 5.0 g melamine were dissolved in 1000 mL ultrapure water (18 MΩ*cm) at 70 °C, and the solution was denoted as solution A. 5.1 g cyanuric acid was dissolved in 2000 mL ultrapure water at 70 °C, and the solution was denoted as solution B. Then solution B was poured into solution A and then maintained for 10 min at 70 °C. The precursor was filtrated, washed with water and dried at 80 °C overnight. The obtained light green powder was placed in a tube furnace and heated at 550 °C for 4 h with a heating rate of 2.5 °C/min under argon gas (100 mL/min). After cooling to ambient temperature, and the obtained catalyst was denoted as Cu-SAs/C_3N_4. The synthesis of Fe-SAs/C_3N_4, Co-SAs/C_3N_4 and Mn-SAs/C_3N_4 were similar to the procedure mentioned above by replacing the Cu source with other metal precursors, while C_3N_4 was prepared without the addition of metal source.

1.3 Synthesis of Cu-NPs/C_3N_4.

For the synthesis of Cu-NPs/C_3N_4, the mass amount of $CuCl_2 \cdot 2H_2O$ was 0.852 g (5 mmol). After solution B was poured into solution A for 10 min, the solution was further dried under stirring until a solid powder was formed. The obtained powder was placed in a tube furnace and heated at 550 °C for 4 h with a heating rate of 2.5 °C/min under argon gas (100 mL/min), and the as-obtained catalyst was denoted as Cu-NPs/C_3N_4. For comparison, Cu/SiO_2 and Cu/Al_2O_3 were prepared with nominal Cu loading amount of 1% by wetness impregnation method, and the samples were calcined at 400 °C in static air for 4 h.

1.4 Characterizations

The loading amount of metal (Cu, Fe, Mn, Co) in the M/C_3N_4 catalysts was determined by an inductively coupled plasma optical emission spectrometer (ICP-OES). X-Ray diffraction (XRD) patterns were recorded on a Rigaku Ultima IV X-ray instrument with Cu Kα (λ=0.154056 nm) radiation at a beam voltage of 40 kV and a beam current of 40 mA, and the scanning speed was 2°/min. The Brunauer Emmett-Teller (BET) specific surface area measurements were determined by a Tristar II system N_2 adsorption/desorption apparatus (Micromeritics Instruments, USA), and the sample were degassed at 120 °C for 5 h before test. The Fourier transform infrared spectroscopy (FT-IR) were recorded on a Thermo Scientific Nicolet 1s1o instrument. The samples were deposited and pressed onto a KBr window and then those were placed in IR cell. Field emission scanning electron microscopy (FESEM) images were obtained with a Zeiss SAPPHIRE Supra 55 system operating voltage at 5 kV. Transmission electron microscopy (TEM) images were obtained on a JEOL JEM-2011 system operating voltage at 100 kV. High-angle annular dark field-scanning transmission electron microscopy (HAADF-STEM) was performed on JEOL ARM300F equipped with double aberration correctors and a cold field emission gun. The chemical state of the catalysts surface elements was characterized by an ESCLAB250 spectrometer, using a monochromatic Al *K*α radiation source (=1486.6 eV). The binding energies (BEs) were calibrated using the C1s peak at 284.8 eV as a reference. The X-ray photoelectron spectroscopy (XPS) were processed by the *Avantage* software, and the ratio of elements with varied valence states was calculated based on the fitted peak areas.

Transition metal (Cu, Fe, Co and Mn) K-edge X-ray absorption spectra (XAS) were performed on the BL14W1 beam line at the Shanghai Synchrotron Radiation Facility (SSRF), operated at 3.5 GeV with injection currents of 210 mA. A Si (111) double-crystal monochromator was used to reduce the harmonic component of the monochrome beam. Cu (Fe, Co and Mn) foils were used as reference sample. The extended X-ray absorption fine structure (EXAFS) raw data were then background-subtracted, normalized and Fourier transformed by the standard procedures with the IFEFFIT package.

The electron paramagnetic resonance (EPR) spectroscopy measurement was performed using an ELEXSYS E5000 spectrometer equipped with a liquid nitrogen cryostat, and 5,5-dimethyl-1-pyrroline-*N*-oxide (DMPO) was used as the radical trap. The samples were dispersed in water to

detect ·CH_3, ·OH and ·OOH radicals. For methane oxidation reaction, the autoclave was firstly charged with 30 mg Cu-SAs/C_3N_4 catalyst, 10 mL ultrapure water, 1.0 mL DMPO (100 mg/mL), 1.0 mL H_2O_2 (40wt%). A sample prior to reaction was removed, filtered and placed in sealed glass tube. The autoclave was purged with 95% CH_4/Ar for three times, and then pressurized to 3 MPa. The reaction mixtures were kept at 25 ^oC for 2 h, and a certain sample was filtered and sealed in a glass tube.

1.5 Catalytic activity Testing

Methane conversion was evaluated in a 50 mL stainless-steel autoclave containing a Teflon liner vessel purchased from Shanghai Yan Zheng Instrument. First, the vessel was charged with 30 mg catalyst, 15 mL H_2O and 5 mL H_2O_2 (40wt%), and then the vessel was flushed with methane and charged to 5~30 bar (95% CH_4 in Ar). The reaction temperature was maintained at 25 ^oC. The reaction products were quickly cooled down in ice bath for 20 min before analysis in order to minimize the loss of volatile products. For the cyclic catalytic test with the same reaction conditions, the stirring paddle were rinsed with water, and the collected rinsing mixture was centrifuged to separate catalyst. The collected catalyst was dried at 80 ^oC before the test for the next run.

1.6 Products Analysis

The gaseous phase products were analyzed by a gas chromatograph (GC-950, Haixin) with an TDX-1 column. The signal was detected by thermal conductivity detector (TCD) and flame ionized detector (FID) with methanizer unit. CO and CO_2 were quantified against a calibration curve constructed from commercial standard. An illustrative GC spectrum was provided in Figure S1.

The liquid products containing methanol (CH_3OH), methyl hydroperoxide (CH_3OOH) and formic acid (HCOOH) were analyzed by 600 M ^1H NMR (Bruker AVIII 600M). After reaction, an aliquot sample (0.5 mL) containing products was mixed with 0.1 mL deuterium oxide (D_2O, Sigma-Aldrich) and 0.1 mL sodium 4,4-Dimethyl-4-silapentane-1-sulfonate (DSS, 6 mM, Tokyo Chemical Industry Co.) as an internal standard. The quantitative analysis of oxygenates was carried out by building standard curves. An illustrative ^1H-NMR spectrum was provided in Figure S2. The oxygenates selectivity (%), turnover frequency (TOF, h^{-1}), the conversion of H_2O_2 and gain (G) factor were calculated using following equations (1-4):

$$\text{Oxygenates selectivity}\,(\%) = \frac{n_{(\text{oxygenated products})}}{n_{(\text{total products})}} \times 100\% \quad (1)$$

$$\text{TOF}\,(h^{-1}) = \frac{n_{(\text{oxygenated products})}}{n_{(\text{metal})} \times h} \quad (2)$$

$$\text{Con}_{H_2O_2}\,(\%) = \frac{n_{(H_2O_2)\text{consumed}}}{n_{(H_2O_2)\text{in}}} \times 100\% \quad (3)$$

$$\text{Gain factor}\,(G) = \frac{n_{(\text{oxygenated products})}}{n_{(H_2O_2)\text{consumed}}} \quad (4)$$

1.7 DFT calculation

Density functional theory (DFT) calculations were performed to optimize the possible active sites in the structure of Cu-N_4. The Gaussian 09 program [1] was used with the B3LYP exchange-correlation functional [2] and the DFT-optimized DZVP2 and DZVP basis sets [3].

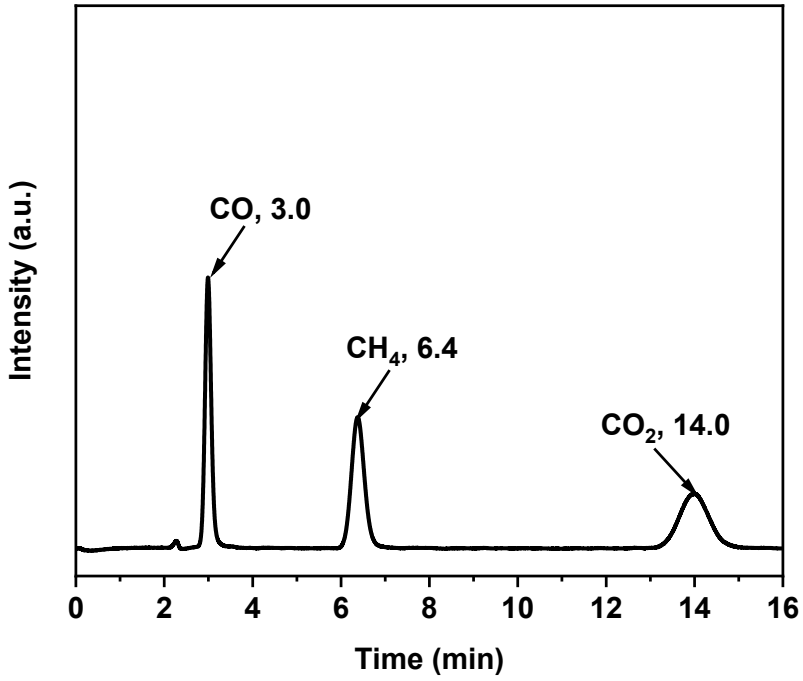

Figure S1. Typical GC-FID spectrum for the identification of CO (**t=3.0 min**), methane (**t=6.4 min**) and CO_2 (**t=14.0 min**).

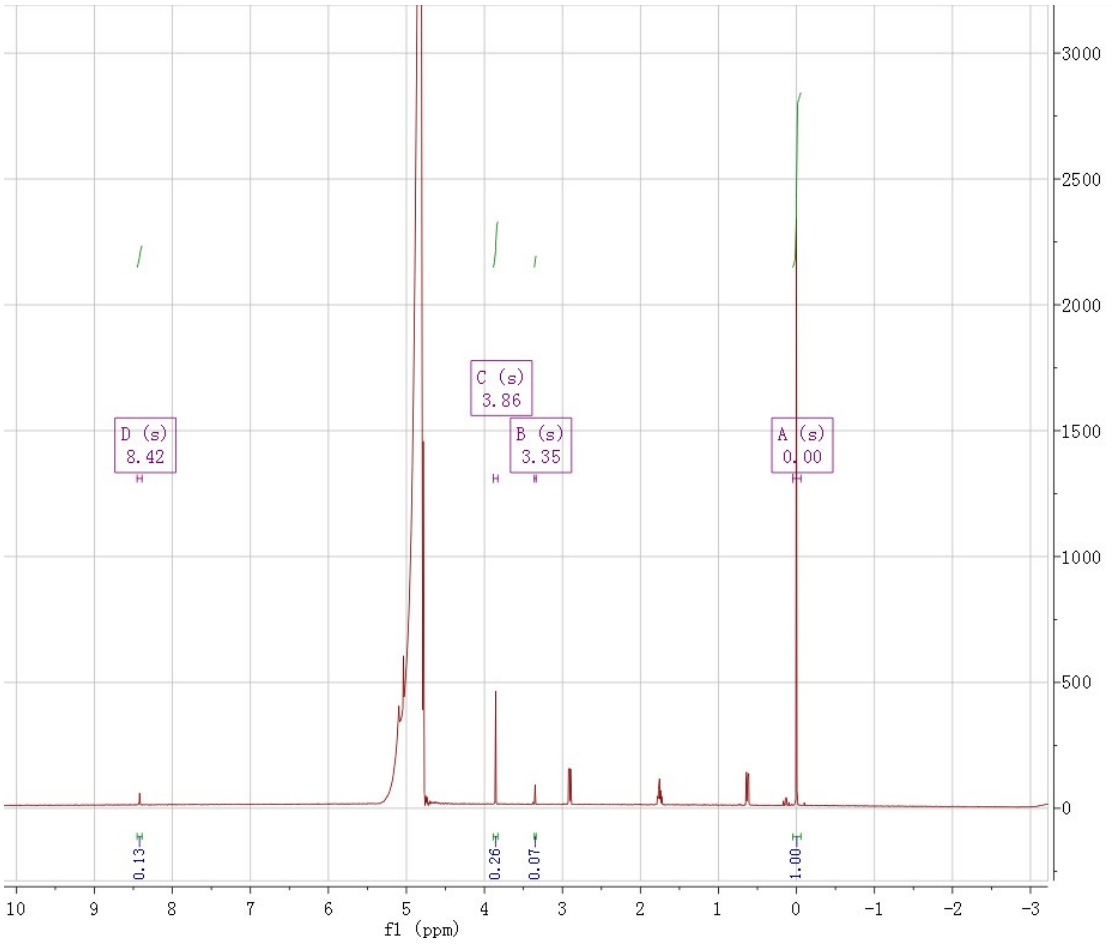

Figure S2. Typical ^{1}H-NMR spectrum for the identification of DSS (**δ=0 ppm**), methanol (**δ=3.35 ppm**), methyl hydroperoxide (**δ=3.86 ppm**) and formic acid (**δ=8.42 ppm**). Resonance at δ=0.6, 1.8 and 2.9 ppm arised from the internal standard. It should be noted that the quantification of CH_3OOH was calibrated by the same curve as that of CH_3OH according to the reported work [4].

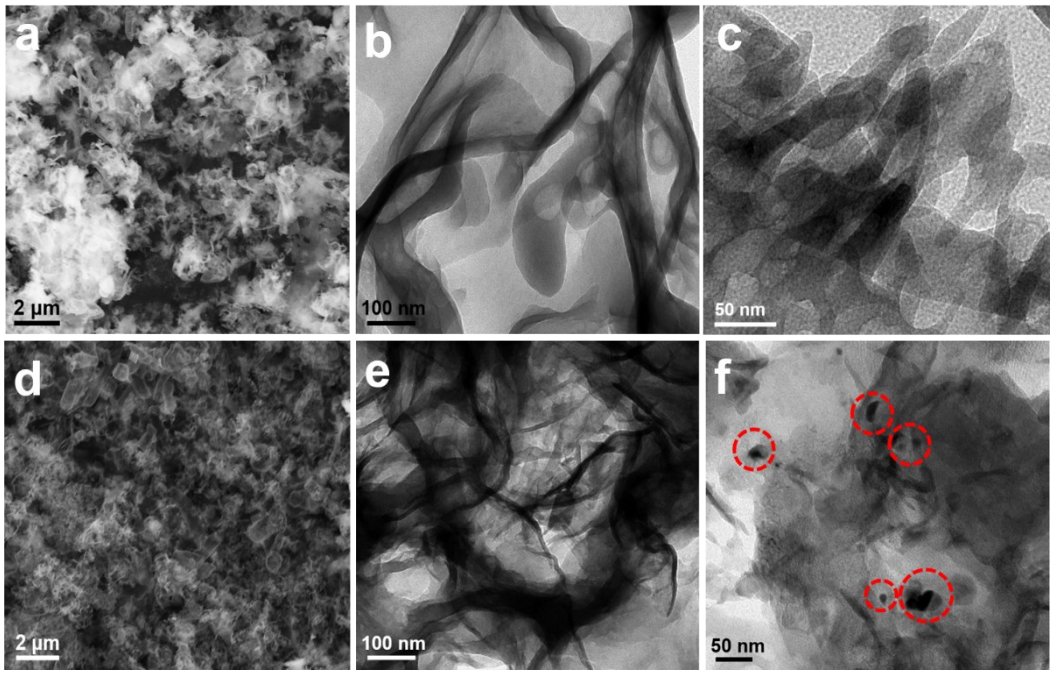

Figure S3. (a) SEM image and (b, c) TEM images of C_3N_4. (d) SEM image and (e, f) TEM images of Cu-NPs/C_3N_4. The representative Cu NPs were highlighted by a red circle.

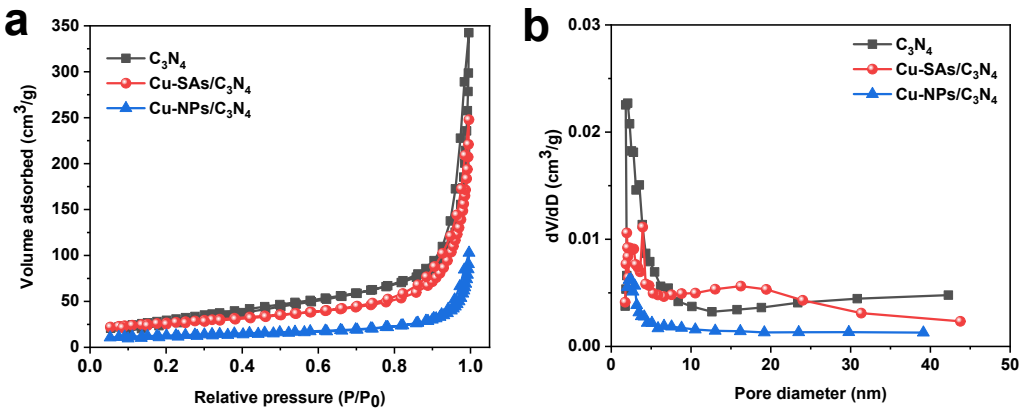

Figure S4. (a) N_2 adsorption and desorption isotherms and (b) Pore size distribution of C_3N_4, Cu-SAs/C_3N_4 and Cu-NPs/C_3N_4 measured at 77 K.

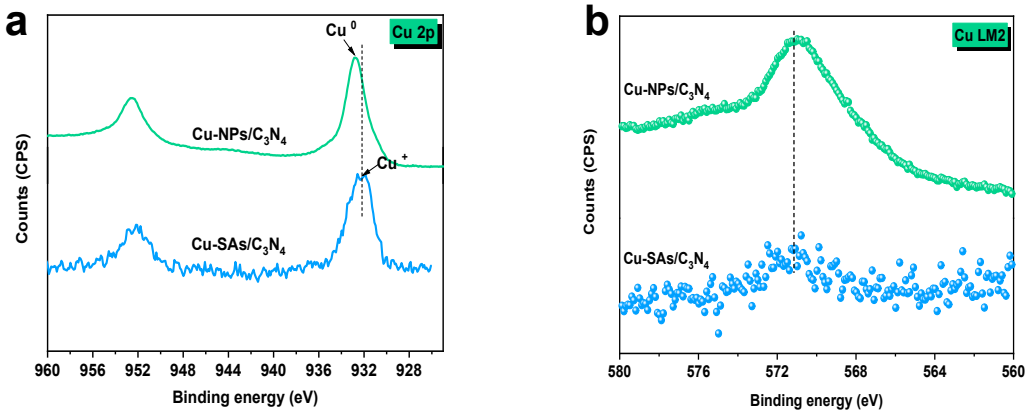

Figure S5. (a) XPS spectra in Cu 2p region and (b) Cu LM2 Auger spectra of Cu-SAs/C_3N_4 and Cu-NPs/C_3N_4. The peaks located at 932.8 eV and 571.1 eV were assigned to Cu^+ species.

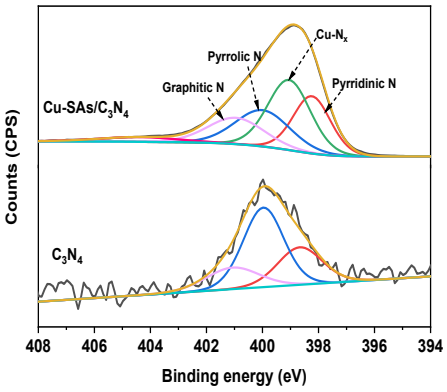

Figure S6. XPS spectra for N 1s region of Cu-SAs/C_3N_4 and C_3N_4. The N 1s XPS spectra of Cu-SAs/C_3N_4 could be spilt into five kinds of nitrogen configurations. Originating from the sp^2-hybridized pyridinic nitrogen atoms in C=N-C, the peak at 398.3 eV demonstrated the successful synthesis of graphite-like C_3N_4. The peaks with binding energy located at 399.1 eV, 400.1 eV, 401.1 eV and 404.1 eV were assigned to nitrogen bonded to copper (Cu-N_x moieties), pyrrolic-N, graphitic-N and oxidized N, respectively. Clearly, for the C_3N_4 matrix, only three peaks could be observed without the presence of two peaks assigned to oxidized graphitic N and the nitrogen bonded to copper.

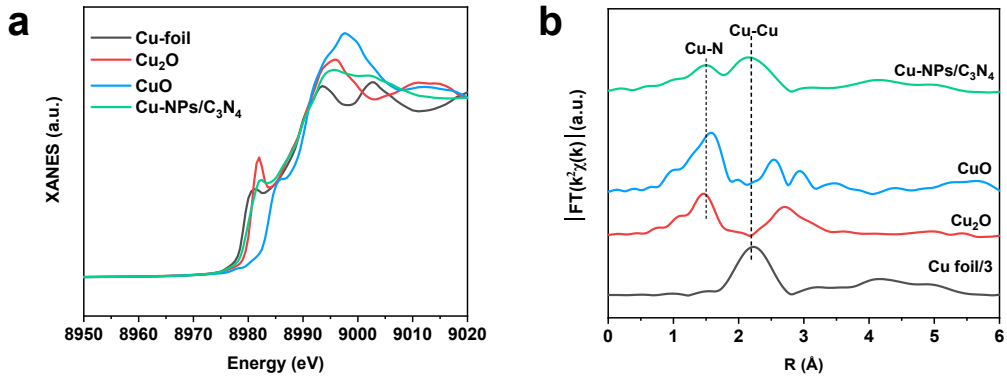

Figure S7. Characterizations of Cu-NPs/C_3N_4. (a) Cu K-edge XANES spectra. (b) Fourier transform (FT) of the Cu K-edge EXAFS.

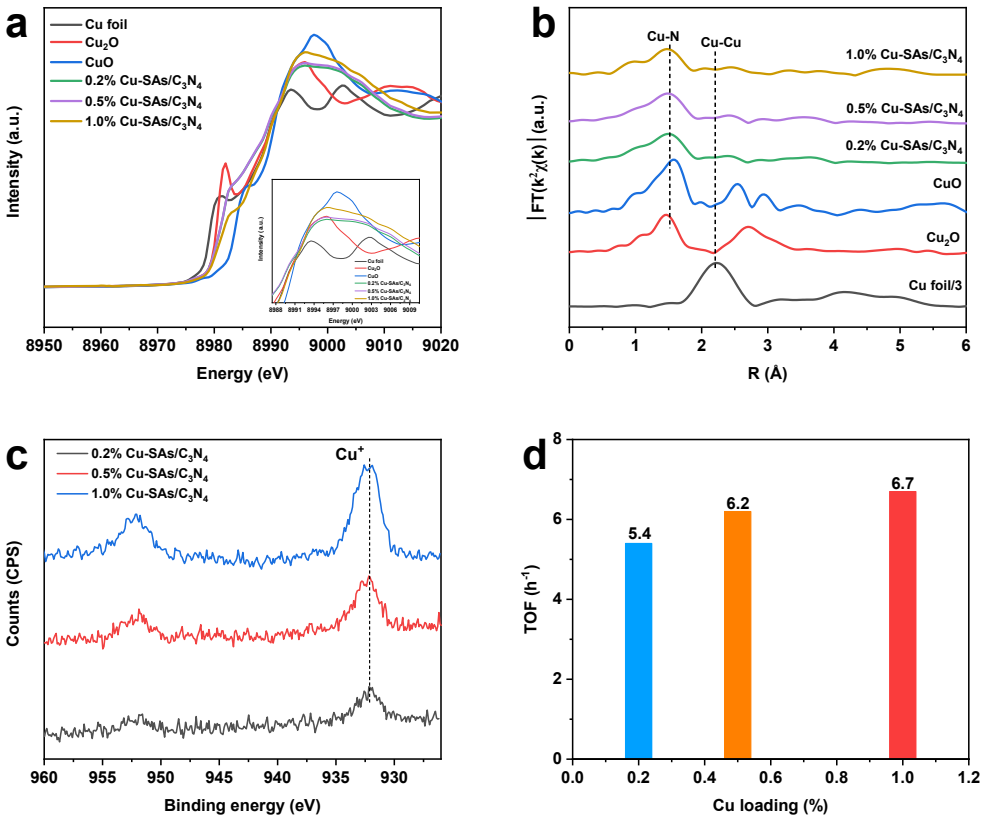

Figure S8. (a) Cu K-edge XANES. (b) FT-EXAFS. (c) XPS spectra of Cu-SAs/C_3N_4 with different Cu loadings. These results revealing that the existence of Cu oxidized state ($1<\delta<2$), and the oxidized state of Cu increased with Cu loadings increased (Figure S8a, the white intensity increased with the Cu loadings increased). (d) TOF versus Cu loadings over the Cu-SAs/C_3N_4 catalyst.

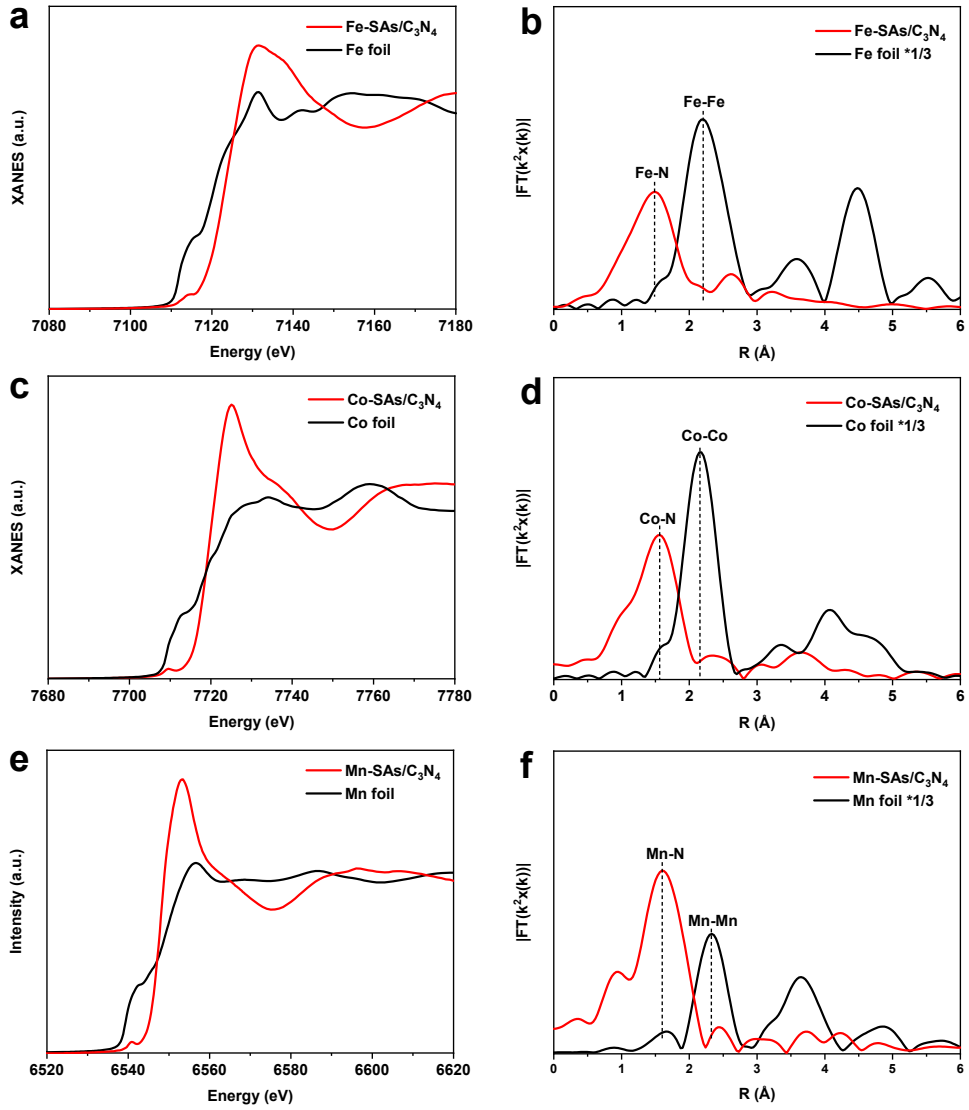

Figure S9. Characterizations of M-SAs/C_3N_4 (M= Fe, Co, Mn) catalyst. (a) Fe K-edge XANES spectra. (b) Fourier transform (FT) of the Fe K-edge EXAFS. (c) Co K-edge XANES spectra. (d) Fourier transform (FT) of the Co K-edge EXAFS. (e) Mn K-edge XANES spectra. (f) Fourier transform (FT) of the Mn K-edge EXAFS.

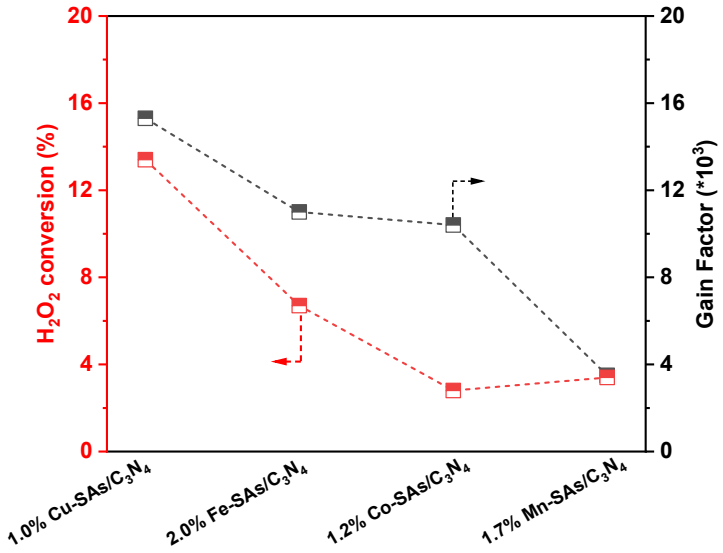

Figure S10. Conversion of H_2O_2 and gain (G) factor during methane oxidation over Cu, Fe, Co and Mn-SAs/C_3N_4 catalysts.

Reaction conditions: 30 mg catalysts, 5 mL 40wt% H_2O_2, 15 mL H_2O, 3 MPa 95% CH_4/Ar, 25 ^oC for 5 h, 1000 rpm.

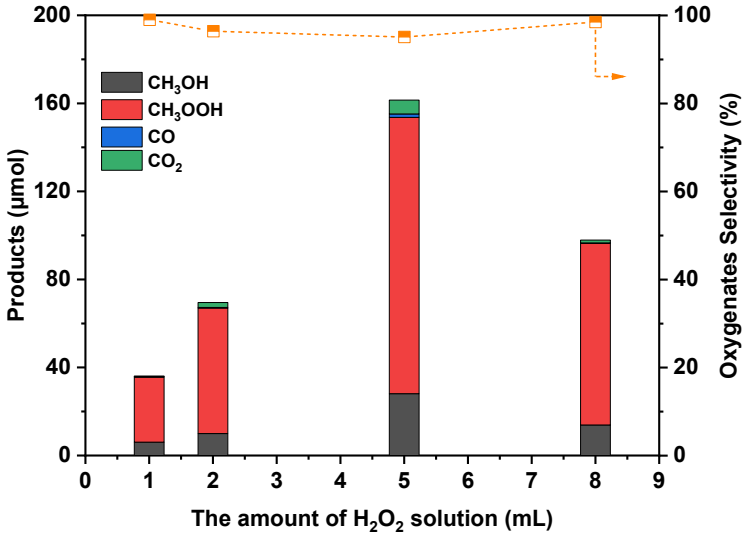

Figure S11. Catalytic performance of the Cu-SAs/C_3N_4 catalyst for methane selective oxidation with different H_2O_2 adding amount.

Reaction conditions: 3 MPa 95% CH_4/Ar, 1~8 mL 40wt% H_2O_2 solution, 20 mL volume in total, 30 mg catalyst, 25 ^oC for 5 h, 1000 rpm.

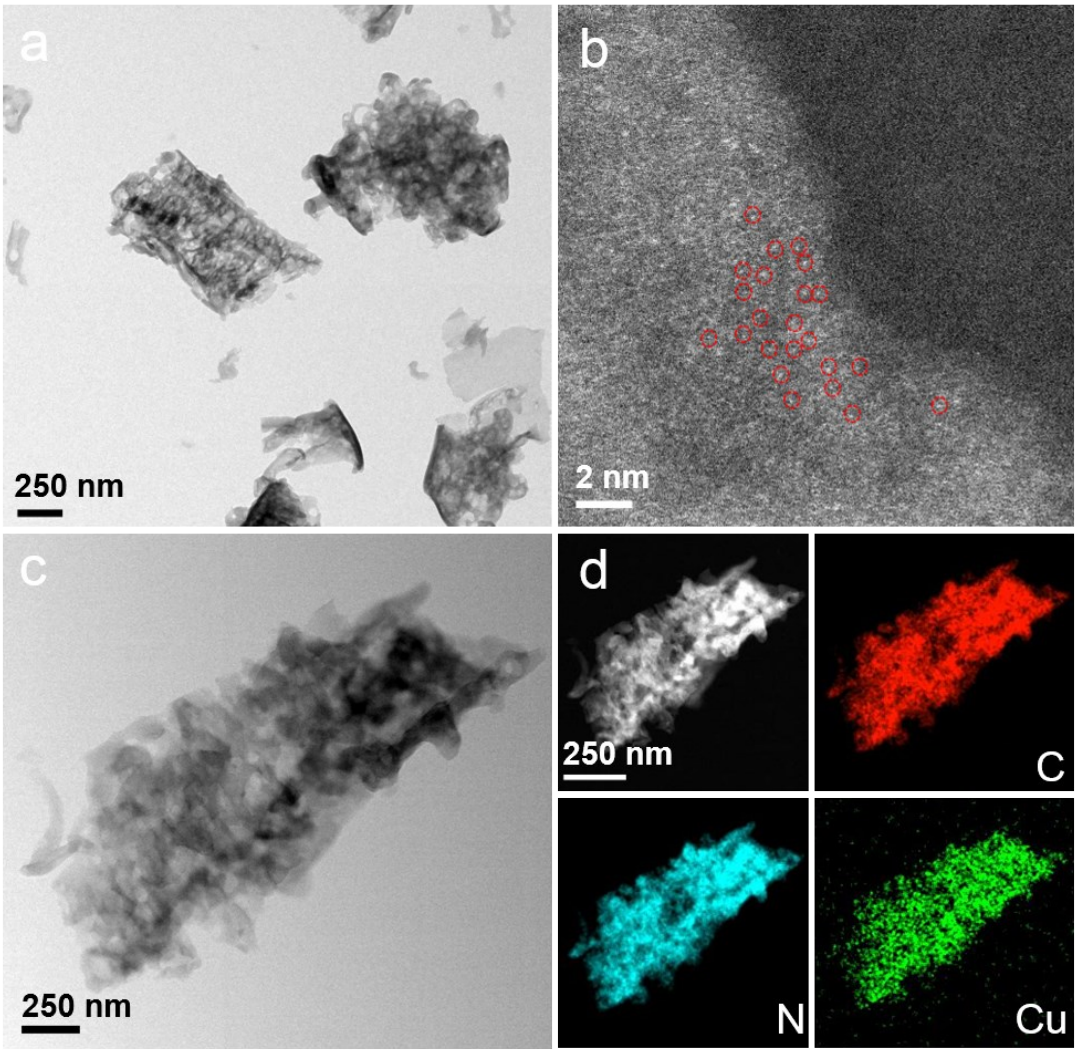

Figure S12. The spent Cu-SAs/C_3N_4 catalyst at 25 °C for 5 h. (a) TEM. (b) AC-HAADF-STEM, the representative Cu single atoms were highlighted by red cycles. (c) STEM and (d) Element mappings.

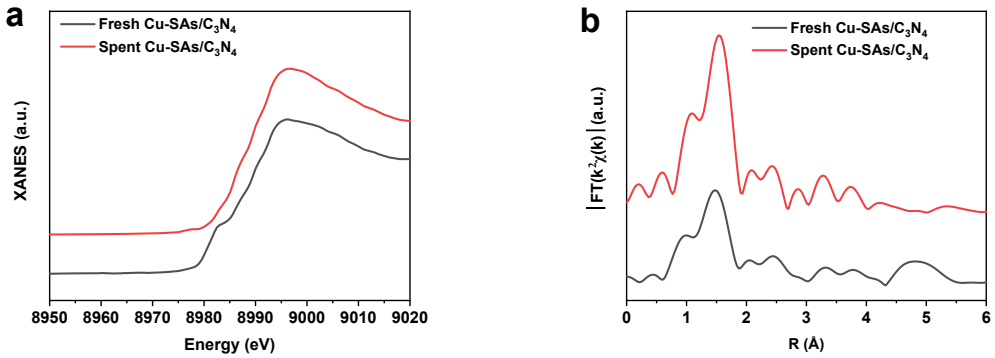

Figure S13. Characterizations of Cu-SAs/C_3N_4. (a) XANES and (b) EXAFS of the fresh Cu-SAs/C_3N_4 and spent Cu-SAs/C_3N_4.

XANES spectrum of the spent Cu-SAs/C_3N_4 exhibited a slightly higher oxidation state of Cu species, indicating the partial oxidation of Cu-N_4 moieties. The EXAFS spectra showed nearly the same characteristics to that of fresh Cu-SAs/C_3N_4. The coordination number of first shell was 4.2 (Table S2) with a slightly increased Cu-N coordination, which was assigned to the interaction between Cu and O atoms during the reaction [5]. The coordination from either Cu-N or Cu-O was undistinguishable in EXAFS. The fitting results of short-range local coordination structure including distance and coordination number suggested that Cu species in the spent Cu-SAs/C_3N_4 remained atomic dispersion.

Table S1. Physical parameters of C_3N_4, Cu-SAs/C_3N_4 and Cu-NPs/C_3N_4.

Samples	Cu loading (%)	S_{BET} [m^2/g]	Pore size [nm]	Pore volume [cm^3/g]
C_3N_4	-	117.8	16.5	0.46
Cu-SAs/C_3N_4	1.0	89.8	15.2	0.34
Cu-NPs/C_3N_4	65.7	42.4	13.1	0.14

Table S2. Structure parameters extracted from the EXAFS fitting.

Sample	Shell	N [a]	R(Å) [b]	$\Delta\sigma^2*10^3$ (Å^2) [c]	R-factor
Cu foil	Cu-Cu	12.0	2.56	/	/
1.0% Cu-SAs/C_3N_4	Cu-N	3.8±1.1	1.95±0.02	4.52±4.57	0.008
1.0% Cu-SAs/C_3N_4 (spent)	Cu-N/O	4.2±1.5	1.97±0.03	4.50±5.31	0.019
0.5% Cu-SAs/C_3N_4	Cu-N	3.7±0.9	1.96±0.02	8.88±3.53	0.002
0.2% Cu-SAs/C_3N_4	Cu-N	3.7±0.8	1.96±0.02	6.24±2.54	0.002
65.7% Cu-NPs/C_3N_4	Cu-N	2.2±0.3	1.92±0.02	6.51±2.16	0.002
	Cu-Cu	3.1±0.4	2.53±0.03	8.67±1.84	

[a] Coordination number; [b] Distance between absorber and backscatter atoms; [c] Debye-Waller factor to account for both thermal and structural disorders; R-factor indicated the goodness of the fit. The obtained S_0^2 of Cu foil was 0.88 and it was fixed in the subsequent fitting of Cu foil K-edge data for the catalyst.

Table S3. Catalytic performance for methane selective oxidation to oxygenates at 25 °C for 5 h.

Entry	Catalysts	Metal loading [%]	Oxygenates [μmol]	TOF [h^{-1}]
1	Cu-SAs/C_3N_4	1.0	153	6.7
2	Cu-SAs/C_3N_4	0.5	71	6.2
3	Cu-SAs/C_3N_4	0.2	25	5.4
4	Cu-NPs/C_3N_4	65.7	65	N.A.
5	Fe-SAs/C_3N_4	2.0	55	1.2
6	Co-SAs/C_3N_4	1.2	37	1.3
7	Mn-SAs/C_3N_4	1.7	15	0.3
8	C_3N_4	0	0	0
9	Cu/SiO_2	1.0	26	1.1
10	Cu/Al_2O_3	1.0	41	1.7

Table S4. Comparison of direct conversion of methane to oxygenates at low temperature

Entry	Catalyst	Temperature [°C]	t [h]	Oxygenates selectivity/%	Production /μmol g^{-1}			TOF [h^{-1}]	Reference
					CH_3OH	CH_3OOH	Total products		
1	1.0% Cu-SAs/C_3N_4	25	2	95	397	2946	3500	11.0	This work
2	2.7% FeN_4/GN	25	10	94	-	-	2300	0.5	*Chem* 2018, 4, 1902
3	CNT@PCN/Ni-SAs(0.68%)	50	10	-	-	-	1574	1.4	*Angew*. Chem. Int. Ed. 2019, 131, 18559
4	1% Cr/TiO_2	25	1	93	50	300	520	2.7	*Angew*. Chem. Int. Ed. 2020, 132, 1232
5	0.3% Rh/ZrO_2	70	0.5	78	31	7	49	3.3	*J. Am. Chem. Soc.* 2017, 139, 17694
6	1% AuPd/TiO_2	50	0.5	90	29	112	157	4.9	*ACS Catal*. 2018, 8, 2567
7	1% AuPd/TiO_2	30	0.5	83	7	39	56	4.3	*Angew*. Chem. Int. Ed. 2013, 52, 1280
8	0.33% Fe/TiO_2	25	3	97	-	-	-	6	*Nat. Catal.* 2018, 1, 889
9	AuPd colloid	50	0.5	88	-	-	-	8.6	*Science* 2017, 358, 223

Table S5. The ICP-OES results for the pristine Cu-SAs/C_3N_4 and Cu-SAs/C_3N_4 after 3 cycles reaction.

Samples	Cu loading (%)
Cu-SAs/C_3N_4	1.0
Cu-SAs/C_3N_4 after 3 cycles reaction	0.99

References

1 M. J. Frisch, G.W. Trucks, H. B. Schlegel, G. E. Scuseria. M. A. Robb, J. R. Cheeseman, G. Scalmani, V. Barone, B. Mennucci, G. A. Petersson, 2009, Gaussian 09, Revision C.01. Gaussian, Inc., Wallingford.

2 A. D. Becke, *J. Chem. Phys*.**1993**, 98, 5648.

3 N. Godbout, D. R. Salahub, J. Andzelm, E. Wimmer, *Can. J. Chem*. **1992**, 70, 560.

4 H. Song, X. G. Meng, S. Y. Wang, W. Zhou, X. S. Wang, T. Kako, J. H. Ye, *J. Am. Chem. Soc*. **2019**, 141, 20507.

5 T. Zhang, D. Zhang, X. H. Han, T. Dong, X. W. Guo, C. S. Song, R. Si, W. Liu, Y. F. Liu, Z. K. Zhao, *J. Am. Chem. Soc.* **2018**, 140:16936-16940.